MITSUBISHI ELECTRIC RESEARCH LABORATORIES
https://www.merl.com

LSTM-Based Modeling and Cross-Correlation Sensitivity Analysis for Heat Pump Refrigerant Distribution

Miyawaki, Kosuke; Qiao, Hongtao; Sciazko, Anna; Shikazono, Naoki

TR2025-141 October 02, 2025

Abstract

This heat pump study introduces a Resonance-Based Sensitivity Analysis (RBSA) framework, which was inspired by the resonant characteristics of LSTM networks to visualize and interpret correlations between output features. First, we developed an LSTM network that predicts the time-series distribution of refrigerant within the system, focusing on refrigerant migration and its nonlinear dependency on the initial distribution in startup operation. A total of nine different datasets were employed, structured as a 3x3 matrix combining three levels of charged refrigerant, incrementing approximately 10wt% of system refrigerant, and three levels of initial refrigerant in evaporator from 30wt% to 70wt%. The prediction by the network achieved a coefficient of determination exceeding 95% in refrigerant distribution against validation data. Subsequently, targeted noise was applied to specific outputs of the trained network to analyze the intensity of inter-feature dependencies, demonstrating the utility of the RBSA approach in capturing causal relationships within the system. We investigated using both spike noise and persistent Gaussian noise in a comparative analysis to evaluate their distinct effects. During sensitivity evaluation with spike noise, we examined noise propagation between features using cross-correlation functions. The analysis revealed that the relationships between parameters maintained physical plausibility, even without an explicit physical model. We then introduced continuous white noise into the refrigerant distribution to examine its propagation effects and map how distribution fluctuations affected system operating parameters. The findings revealed that variations in refrigerant distribution substantially affect operating parameters such as mass flow rate, compressor input and condenser and evaporator capacity.

International Journal of Refrigeration 2025

Mitsubishi Electric Research Laboratories, Inc.
201 Broadway, Cambridge, Massachusetts 02139

LSTM-Based Modeling and Cross-Correlation Sensitivity Analysis for Heat Pump Refrigerant Distribution

Kosuke Miyawaki[a], Hongtao Qiao[b], Anna Sciazko[c], Naoki Shikazono[c]

a Advanced Technology R&D Center, Mitsubishi Electric Co., Amagasaki, Hyogo, Japan
b Mitsubishi Electric Research Laboratories, Cambridge, MA, USA
c Institute of Industrial Science, The University of Tokyo, Meguro-ku, Tokyo, Japan

Abstract

This heat pump study introduces a Resonance-Based Sensitivity Analysis (RBSA) framework, which was inspired by the resonant characteristics of LSTM networks to visualize and interpret correlations between output features. First, we developed an LSTM network that predicts the time-series distribution of refrigerant within the system, focusing on refrigerant migration and its nonlinear dependency on the initial distribution in startup operation. A total of nine different datasets were employed, structured as a 3x3 matrix combining three levels of charged refrigerant, incrementing approximately 10wt% of system refrigerant, and three levels of initial refrigerant in evaporator from 30wt% to 70wt%. The prediction by the network achieved a coefficient of determination exceeding 95% in refrigerant distribution against validation data. Subsequently, targeted noise was applied to specific outputs of the trained network to analyze the intensity of inter-feature dependencies, demonstrating the utility of the RBSA approach in capturing causal relationships within the system. We investigated using both spike noise and persistent Gaussian noise in a comparative analysis to evaluate their distinct effects. During sensitivity evaluation with spike noise, we examined noise propagation between features using cross-correlation functions. The analysis revealed that the relationships between parameters maintained physical plausibility, even without an explicit physical model. We then introduced continuous white noise into the refrigerant distribution to examine its propagation effects and map how distribution fluctuations affected system operating parameters. The findings revealed that variations in refrigerant distribution substantially affect operating parameters such as mass flow rate, compressor input and condenser and evaporator capacity.

Nomenclature

b	Bias, -
c	Cell state, -
CCF	Cross correlation function, -
d	deviation
D_{DTW}	Dynamic time warping distance
D_{norm}	Normalized dynamic time warping distance
$\mathbb{e}_k$	the standard basis vector selecting k-th dimension, -
f	Forget gate, -
g	Update gate, -
h	Hidden state, -
H	Enthalpy, kJ/kg
i	Input gate, -
j	Time step, -
k	Output dimension, -
L	Length of the warping path, -
$\mathcal{N}$	Normal distribution, -
o	Output gate, -

q	Quality, -
R^2	Coefficient of determination, -
T, t	Time, sec
$\mathbb{v}$	the perturbation direction, -
W	Weight matrix, -
x	Input vector, -
y	Output vector, -
$\overline{y_i}$	Time averaged output at i, -
$\tilde{y}$	Noise added output vector, -

Greek symbol

δ	Spike perturbation, -
Δ	perturbation
ε	Gaussian noise, -
σ	Variance, -
τ	Lag, sec

Subscripts

fc	Fully connected
$q = 0$	Saturated liquid
$q = 1$	Saturated vapor
raw	Raw data

1. Introduction

Air conditioning constitutes a major portion of energy consumption, with thermal and fluid management technology serving as a key pathway to energy conservation [1-3]. Heat pump systems represent one of the most efficient heating and cooling solutions, with rapid market growth worldwide. However, their complex system design requires extensive knowledge of thermal and fluid sciences, which limits widespread adoption [4, 5]. The systems demand sustained development efforts to improve performance metrics like coefficient of performance while maintaining reliability, which often increases system costs. The primary challenge in heat pump system design arises from the complex phenomena in multiphase refrigerant. Although many studies have contributed to revealing their specific phenomena [6-11], at least thus far, many aspects of multiphase refrigerant flow remain unresolved, and conventional prediction methods which most rely on integrated physical models, face challenges in comprehensively capturing these complex dynamics. For instance, gas-liquid phase flow involves various complex phenomena which necessitate cautious design to prevent system malfunction, in particular, refrigerant migration during startup [12-15]. Nevertheless, few studies have comprehensively analyzed the influence of the initial refrigerant distribution on system performance. One contributing factor is the difficulty in transiently and accurately measuring the refrigerant distribution. A conventional technique for quantifying refrigerant distribution is the quick-closing valve (QCV) method [16], in which a valve in the flow path is rapidly closed to sample the fluid. Although this method yields reliable direct measurements, its application during transient operation interferes with the flow, rendering it unsuitable for in-situ monitoring under actual operating conditions. Analytically, the migration of the refrigerant has been investigated through the development of physical models for components, which are validated by comparing model predictions with instantaneous experimental data [13]. While the analytical approach obviates the requirement for sampling procedure, it is hampered by a substantial computational cost [17]. In recent years, data-driven predictive approaches have evolved as a method for understanding complex phenomena [18-21]. This technology enables a reduction in testing workload by extrapolating untested data from multiple test datasets, facilitates the visualization of phenomena that are difficult to observe visually and promotes understanding of these phenomena through integration with measurement techniques. Furthermore, it accelerates prediction by omitting calculations through learning from analytical data and improves prediction accuracy by reproducing unformulated phenomena, thereby advancing the foundation technologies of both testing and analysis aspects.

To predict transient phenomena, it is necessary to learn certain historical information. However, since a system may trace countless operating histories, there is concern that learning with specific historical data will reduce prediction accuracy for other conditions. Therefore, in this study, we selected a long-short term memory (LSTM) network [22], which is one of the recurrent neural networks (RNN). LSTM is an attractive method for learning and predicting time sequence dependencies. Table 1 summarizes previous LSTM-based studies in energy fields. Palagi et al. [23] compared the accuracy of deep learning models by predicting the non-stationary operation of an organic Rankine cycle and reported that LSTM provides outstanding accuracy. Laib et al. [24] and Bouziane and Khadir [25] used a modified LSTM to predict energy consumption or generation and reported improvement in accuracy compared to potential candidates. The networks excel not only in identifying superficial input-output relationships, but also comprehensively understanding intricate the dynamic characteristics of the system by their ability to retain past information and capture dynamic changes. Lyu et al. [26] adopted LSTM to predict particle migration in fuel cell microstructure to design performance and lifespan. In the HVAC field, in addition to the studies of

LSTM to predict system performance [27-29], frosting phenomena in outdoor unit heat exchanger were predicted by Eom et al. [30], and flooding phenomena of lubricant in gas pipe was studied by Jeong et al. [31]. Their contributions revealed that LSTM method can successfully demonstrate the operation derived from their subject phenomena. However, a key limitation remains: the black-box nature of neural network models poses challenges for practical system design and optimization. As pointed out in various fields, a major drawback of data driven models is that their derivation process becomes a black box [32, 33]. This makes it difficult to establish guidelines on how to design and apply specific design parameters compared with model-driven approaches in white or grey box [34, 35] models. To overcome this barrier, we devised a method in which the architecture of a network is reconfigured to inject controlled noise into a specific feature, thereby enabling us to observe and analyze the corresponding output response. Similar to stochastic resonance in physical systems, where noise can enhance weak signal detection [36, 37], LSTM networks demonstrate enhanced pattern recognition capabilities when processing noisy temporal data through their specialized gating mechanisms. This parallel is particularly evident in applications where minimal background noise improves the neural representation of temporal patterns, as observed in both natural and artificial systems [38–40]. In this study, refrigerant migration in transient operation in a heat pump system is examined. We employed an LSTM neural network and trained the network using simulated results under various initial distribution of the refrigerant and charge levels. Following the verification of the network, we introduced perturbations to the trained network and developed a method that analyzes the sensitivity. By confirming that these results align with established knowledge, we evaluated the practicality of LSTM for extracting design guidelines rather than merely discussing network accuracy.

Table 1 Previous studies on LSTM based analysis in power generation and consumption.

Authors	Network Type	System type	Objectives	Phenomena
Palagi et al. [23]	Feed Forward Simple RNN LSTM	Organic Rankine cycle	Thermodynamics	Load fluctuation
Laib et al. [24]	LSTM x MLP	Nation wide gas demand	Gas consumption	Weather, cultural events
Bouziane and Khadir [25]	LSTM	Power generation (Multiple sources)	Power efficiency, CO_2 emission	Seasonal demand, generation
Lyu et al. [26]	LSTM x DEIS	Fuel cell	Voltage	Degradation (Particle migration)
Zou et al. [27]	LSTM×DRL	Heat pump	Sensor data	Daytime operation
Lahariya et al. [28]	phyLSTM	Evaporative cooling system	Basin temperature	Fan power dependence
Kong et al. [29]	ANN K-nearest neighbors LSTM	Smart grid city (Hot water system)	Energy consumption	Residence behaviour
Eom et al. [30]	FCDNN CNN LSTM	Heat pump	Capacity, power	Frosting
Jeong et al. [31]	LSTM×BN	Heat pump	Oil film thickness	Flooding
This study	LSTM	Heat pump	Thermodynamics	Refrigerant

2. Neural Network Models

2.1. LSTM unit

The LSTM unit shown in Fig. 1 consists of a storage cell and three gates (input gate, forget gate, and output gate) that control the cell state. At time t, x_t, h_{t-1} and c_{t-1} are the inputs, and h_t and c_t are the outputs. The input gates are selected to propagate only the necessary information from the current input information. The forget gate determines the information to be inherited from the past. The output gate selects the signal to propagate. The cell and each gate are represented by the following equation.

$$i_t = \sigma(W_{x,i}x_t + W_{h,i}h_{t-1} + b_i) \quad (2\text{-}1)$$

$$f_t = \sigma(W_{x,f}x_t + W_{h,f}h_{t-1} + b_f) \quad (2\text{-}2)$$

$$g_t = \tanh(W_{x,g}x_t + W_{h,g}h_{t-1} + b_g) \quad (2\text{-}3)$$

$$o_t = \sigma(W_{x,o}x_t + W_{h,o}h_{t-1} + b_o) \quad (2\text{-}4)$$

$$c_t = f_t \circ c_{t-1} + i_t \circ g_t \quad (2\text{-}5)$$

$$h_t = o_t \circ \tanh(c_t) \quad (2\text{-}6)$$

where σ is the sigmoid function, $\circ$ is the Hadamard product (element-wise multiplication), and W and b are the weight matrix and bias, respectively. The stationary character t denotes time, and f, g, i, o denote each gate in the network, forget, update, input, and output gate, respectively. These weights and biases are determined by learning so that the output and input data are minimized. The final output of the network at time *t* is computed as:

$$y_t = W_{\mathrm{fc}}h_t + b_{\mathrm{fc}} \quad (2\text{-}7)$$

where W_{fc} represents the weight matrix connecting the final hidden state to the output, and b_{fc} represents the output bias in fully connected layer, respectively.

2.2. Network construction

The network illustrated in Fig. 1 comprises two LSTM layers serving as intermediate layers. The first LSTM layer, which receives the input, consists of 400 hidden units and outputs an equivalent number of features. To improve generalization performance, a dropout layer is inserted immediately after the first LSTM layer, where units are randomly dropped with a probability of 0.2 during training. The second LSTM layer is also composed of 400 hidden units, and its outputs are passed to a subsequent fully connected layer to produce the final output. Table 2 provides detailed information about the network architecture.

2.3. Network optimization

LSTM's distinctive feature lies in its ability to selectively retain or discard input information at each time step, thereby facilitating the retention of past history. In constructing the network, standardization procedures were performed to the chosen input and output features. The raw simulation data are normalized via z-score normalization prior to being used for network training and analysis. The means and standard deviations for both the inputs and outputs are computed using the aggregated data. Then, each time step data is normalized accordingly.

$$\mu_{x^{(i)}} = \frac{1}{T}\sum_{\mathrm{i}=1}^{T} x_{\mathrm{raw}}^{(i)}(t), \quad (2\text{-}8)$$

$$\bar{\sigma}_{x^{(i)}} = \sqrt{\frac{1}{T-1}\sum_{t=1}^{T}\left(x_{\text{raw}}^{(i)}(t) - \mu_{x^{(i)}}\right)^2}, \tag{2-9}$$

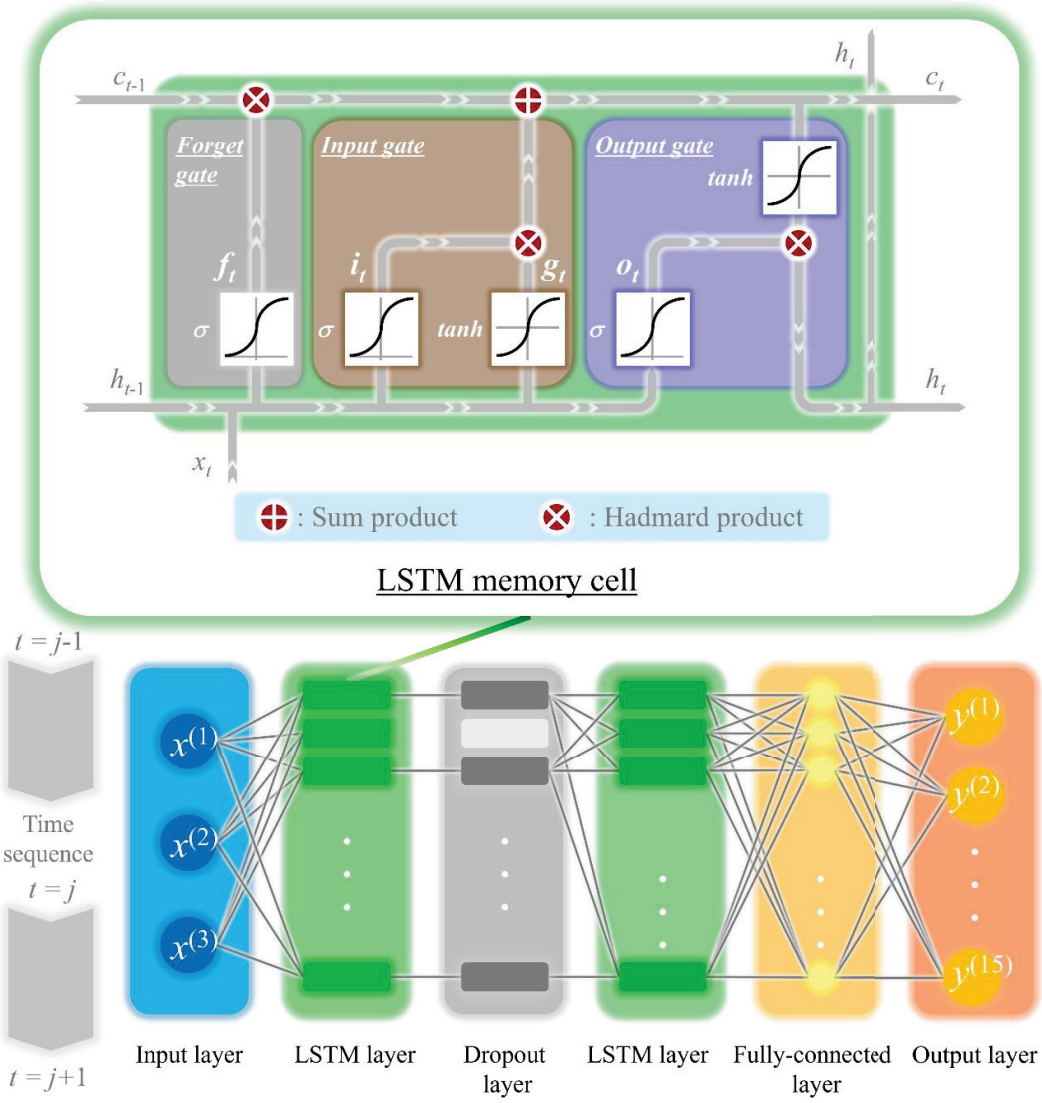

Fig. 1. Schematic picture of LSTM memory cell.

Table 2 Hyperparameter settings for the network.

Layer	Parameter	Value
Input	Number of input features	3
First LSTM	Number of hidden units	400
Dropout	Dropout rate	0.2

Second LSTM	Number of hidden units	400
Fully connected	Number of output features	15

$$x^{(i)}(t) = \frac{x_{raw}^{(i)}(t) - \mu_{x^{(i)}}}{\bar{\sigma}_{x^{(i)}}}. \quad (2\text{-}10)$$

After standardization, the data are partitioned into training and testing sets. This implementation ensures that features have a mean of zero and unit variance, which helps to improve overall predictive performance in various range of parameters. The Adam optimization algorithm [41] was employed for network training, with an initial learning rate of 0.005 that was reduced by a multiplicative factor of 0.2 every 125 epochs, over a total of 1600 epochs. Since the learning rate schedule is not the primary focus of this discussion, readers are referred to [41, 42] for further details; for additional insights, see the seminal work by Smith [43]. Training was conducted using the MATLAB Deep Learning package [44].

2.4. Analysis in trained network

Sensitivity analysis using perturbation methods are applied to perform investigation in amplitude and duration of the impact in output features. Perturbations to the input can be analyzed by instantaneously or continuously modifying the network's input. However, analyzing the sensitivity of other features to perturbations in a specific output requires a nuanced approach. In this study, we introduced instantaneous or continuous noise into the hidden layers, which convey short-term memory within the network, to investigate the temporal propagation of these perturbations.

2.4.1 Spike noise analysis

To evaluate how perturbations in the network's output affect its temporal behavior, a small perturbation δ is introduced at time step *j* for a specific output dimension *k*:

$$\tilde{y}(t) = \begin{cases} y(t) + \delta^{(k)} & \text{if } t = j \\ y(t) & \text{otherwise} \end{cases}. \quad (2\text{-}11)$$

This perturbed output is propagated backward into the network by solving the inverse transformation:

$$\tilde{h}_j = h_j + {W_{fc}}^{-1}\big(\tilde{y}(t) - y(t)\big). \quad (2\text{-}12)$$

To ensure the perturbation is reflected proportionally in the latent space, a linear inverse transformation is used. The perturbed hidden state $\tilde{h}_j$ is then used to compute future hidden states:

$$\tilde{h}_{j+1} = o_{j+1}(\tilde{h}_j) \circ \tanh(f_{j+1}(\tilde{h}_j) \circ c_j + i_{j+1}(\tilde{h}_j) \circ g_{j+1}(\tilde{h}_j)). \quad (2\text{-}13)$$

The deviation in the final output is computed as:

$$d(t) = \tilde{y}(t) - y(t). \quad (2\text{-}14)$$

All LSTM gates and memory updates involve bounded nonlinearities, which inherently limit the propagation of unbounded growth in perturbation influence, thus contributing to overall numerical stability. By iterating over all *t*, we observe propagation level and duration of perturbation in output feature. The operation sensitivity of a sudden, short-duration perturbation would suggest optimal controls of system actuators.

2.4.2 Gaussian noise analysis

To examine the influence of perturbations, additive white gaussian noise ε is applied as continuous Gaussian noise $\varepsilon(t)$ to a specific output component to the entire time sequence.

$$\tilde{y}(t) = y(t) + \varepsilon(t), \quad (2\text{-}15)$$

$$\varepsilon(t) \sim \mathcal{N}(0, \sigma^2 \mathbb{e}_k \mathbb{e}_k{}^{\top}), \tag{2-16}$$

where σ is the perturbation amplitude, $\mathbb{e}_k$ is the standard basis vector. The perturbation induced in the hidden state is then expressed as:

$$\Delta h_j = \tilde{h}_j - h_j = W_{fc}{}^{-1}\big(\varepsilon(t)\big), \tag{2-17}$$

$$\Delta h_j \sim \mathcal{N}\big(0, \sigma^2 W_{fc}{}^{-1} \mathbb{e}_k \mathbb{e}_k{}^{\top} (W_{fc}{}^{-1})^{\top}\big). \tag{2-18}$$

If we the perturbation direction $\mathbb{v}_k$as:

$$\mathbb{v}_k = W_{fc}{}^{-1} \mathbb{e}_k, \tag{2-19}$$

then the hidden state perturbation Δh_j can be described as follows:

$$\Delta h_j \sim \mathcal{N}(0, \sigma^2 \mathbb{v}_k \mathbb{v}_k{}^{\top}). \tag{2-20}$$

This indicates that Δh_j also follows a Gaussian distribution. This formulation enables modeling interdependencies between outputs, offering richer insight into how coupled outputs jointly affect internal dynamics.

2.5 Data regression

2.5.1 Root Mean Squared Error (RMSE)

RMSE is a widely used metric for evaluating predictive accuracy.

$$RMSE = \sqrt{\frac{1}{T}\int_{t_0}^{t_1}[y_k(t) - \widehat{y_k}(t)]^2 dt}, \tag{2-21}$$

where y_i represents the true values, $\widehat{y_i}$ denotes the predicted values, T is time duration of error evaluation where,

$$T = t_1 - t_0. \tag{2-22}$$

While RMSE provides a simple and interpretable measure of overall prediction error, it is highly sensitive to outliers, as the squared error term disproportionately amplifies the impact of large deviations. In the context of time series data, where transient anomalies or phase shifts may occur, RMSE may not accurately reflect the temporal or structural similarity between sequences.

2.5.2 Coefficient of determination (R^2)

To quantitatively compare the prediction errors across multiple network outputs Coefficient of determination (R^2) is applied to enable a scale-independent evaluation of prediction accuracy across different output variables. The coefficient of determination for specific output ${R_k}^2$ is computed as:

$${R_k}^2 = 1 - \sqrt{\frac{1}{T}\int_{t_0}^{t_1}[y_k(t) - \widehat{y_k}(t)]^2 dt}/{\bar{\sigma}_k}^2, \tag{2-23}$$

$\bar{\sigma}_k$ is the time averaged variance of the testing data, defined as:

$${\bar{\sigma}_k}^2 = \frac{1}{T}\int_{t_0}^{t_1}[y_k(t) - \overline{y_k}]^2 dt, \tag{2-24}$$

with the time average mean of the true data:

$$\overline{y_k} = \frac{1}{T}\int_{t_0}^{t_1} y_k(t) dt. \tag{2-25}$$

Using R^2 instead of Root Mean Square Error (RMSE) is intended to compare the prediction accuracy in various parameters. Each parameter has a different magnitude, and it is profitable to preserve scale invariance. Therefore, normalization by the variance of corresponding output is applied to correlatively evaluate prediction accuracy of each parameter.

2.5.3 Dynamic Time Warping (DTW)

DTW is a non-linear alignment-based measure that accounts for temporal shifts and local distortions in sequence alignment [45]. The DTW distance is computed by minimizing the cumulative cost over all valid warping paths.

$$D_{\mathrm{DTW}}(y_k, \widehat{y_k}) = min\sum_{(m,n)\in W}\sqrt{(y_{k,m} - \widehat{y_{k,n}})^2}, \tag{2-26}$$

where $W = \{(y_{k,l} - \widehat{y_{k,l}})\}_{l=1}^{L}$ is the warping path, which is a sequence of index pairs that defines the alignment between the two sequences, subject to boundary, monotonicity, and step size constraints. To normalize this distance and allow comparison across sequences of varying length or sampling rates, we define the normalized DTW distance as:

$$D_{\mathrm{norm}}(y_k, \widehat{y_k}) = \frac{D_{\mathrm{DTW}}(y_k, \widehat{y_k})}{L}, \tag{2-27}$$

where L is the length of the warping path.

2.5.4 Cross-correlation function (CCF)

To assesses the similarity and possible lag relationship between two time series signals enabling detection of time-shifted dependencies, the cross-correlation function (CCF) is applied between the prediction and testing data for evaluating time lags and shapes in time-series. In addition, it is applied between the additive noise in specific feature and its response in other features for evaluating the causality and response time delays.

To assess potential phase lag between two different signals, the normalized CCF is employed:

$$CCF_k(\tau) = \frac{\int_{t_0}^{t_1}[y_k(t)-\overline{y_k}][\hat{y}_k(t+\tau)-\overline{\hat{y}_k}]dt}{\int_{t_0}^{t_1}[y_k(t)-\overline{y_k}]^2 dt \int_{t_0}^{t_1}[\hat{y}_k(t)-\overline{\hat{y}_k}]^2 dt}, \quad (2\text{-}28)$$

The normalization constrains the CCF values in the range [-1, 1] to render the scale invariant and thus improve the comparability and the interpretability.

A value near 1 indicates a strong positive correlation, while a value near −1 indicates a strong negative correlation. In the context of transient prediction, the lag τ_{max} that maximizes $CCF_k(\tau)$ is used to quantify the phase alignment between the evaluating features.

3. Validation case

3.1 Refrigerant circuit specifications

Figure 2 shows a schematic diagram of the refrigerant circuit used to generate the training data and the circuit specifications used is shown in Table 3. It is a simplified analysis circuit connected with sample elements. In this study, training and verification data was prepared with the simulation model according to Qiao et al. [46, 47] These models are augmented by a set of empirical relations describing the heat transfer and frictional pressure drops, as listed in Table 4. For the heat exchanger analysis, the performance of each tube was analyzed separately, and each tube was associated with different refrigerant and air parameters. In the evaporator and the condenser, the flow direction of air and refrigerant are co-current and counter current, respectively. Frost formation was not considered in the analysis. These models were implemented in the Modelica language using Dymola 2023x environment [54].

3.2 Feature selection

The input data for LSTM network consisted of compressor frequency and charge amount of refrigerant as well as the initial refrigerant concentration in the evaporator In other words, within a single dataset, the compressor frequency was a variable, while the refrigerant charge amount and the initial refrigerant distribution were constants, with the latter constants taking different values between datasets, as explained in the next section. The output data included refrigerant flow rate, compressor input power, evaporation and condensation capacity, saturated discharge and suction temperature, discharge and suction temperature, discharge enthalpy of compressor, evaporator and condenser, and refrigerant distribution (evaporator, condenser, gas extension pipe, and liquid extension pipe). The selection of the output features is based on its representation in the Moller diagram of refrigerant cycle. The inclusion of refrigerant temperature, saturation temperature, and enthalpy simultaneously in the training data aims to enable the network to implicitly account for differences in phase states during training, as the network does not inherently learn the thermophysical properties of the refrigerant. By incorporating these variables as features, we aim to enable the network to implicitly account for differences in phase states during training.

3.3 Data preparation

In this study, simulation data with compressor control as shown in Fig. 2 and various initial distributions of refrigerant with charged refrigerant conditions as shown in Table 5 were prepared for testing and training. The operational data used for training the model involved a compressor frequency ramp-up from startup to 1000 seconds at a uniform increasing rate of 6×10^{-2} Hz/s until reaching 60 Hz, maintained for 500 seconds, followed by a ramp-down at the same rate until shutdown. For the refrigerant conditions in the dataset, the refrigerant amount was prepared in increments of 0.2 kg, ranging from 1.9 kg to 2.5 kg, which is approximately 10wt% of the system refrigerant amount. The initial refrigerant distribution in the evaporator was prepared in increments of 20 wt%, ranging from 30 wt% to 70 wt%. For the validation data, the system refrigerant amount was set to 2.3 kg, and the initial refrigerant amount ratio in the evaporator was set to 60 wt%. The validation of the model's performance was conducted using a separate dataset not included in the training phase, thereby ensuring the robustness and reliability of the neural network's learning performance. Each output data point was organized at one-second interval for subsequent analysis.

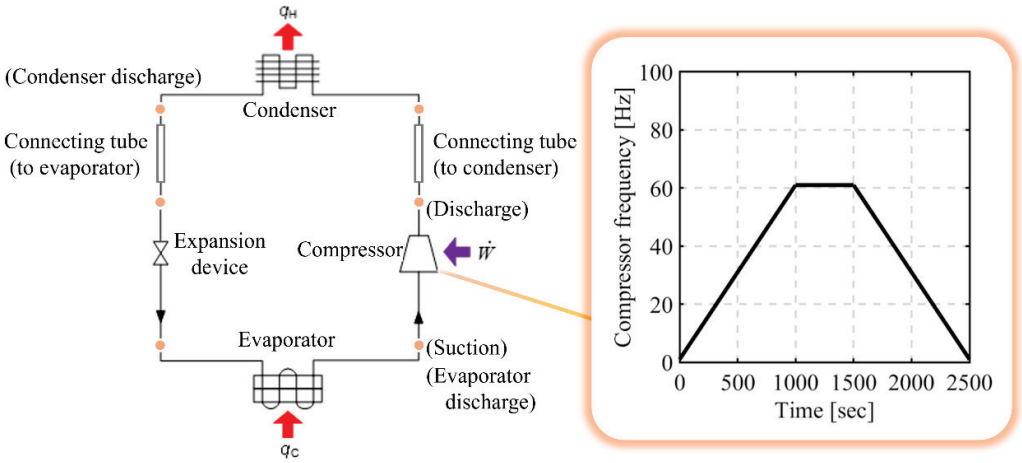

Fig. 2. Schematic picture of refrigerant cycle and compressor frequency control.

Table 3 Refrigerant cycle models.

Element	Parameters	Unit	Value
System	Working fluid	-	R32
Compressor	Stroke volume	cc.	20
Condenser	Tube volume	m^3	1.4×10^{-3}
	Inlet air DBT	ºC	20
	Air flow rate	m^3 /min	55
Evaporator	Tube volume	m^3	3.2×10^{-3}
	Inlet air DBT	ºC	7.0
	Inlet air WBT	ºC	6.0
	Air flow rate	m^3 /min	122
Expansion valve	Cv.	-	0.06
Connecting tube (To condenser)	Inner diameter	mm	8
	Length	m	5
Connecting tube (To evaporator)	Inner diameter	mm	6
	Length	m	5

Table 4 Correlations used in the heat exchanger models.

Modeled phenomena	Applied model
Single-phase heat transfer	Dittus & Bolter [48]
Condensation heat transfer	Dobson & Chato [49]
Evaporation heat transfer	Gungor & Winterton [50]
Single-phase pressure drop	Blasius (Incropera & DeWitt [51])
Condensation pressure drop	Lockhart & Martinelli [52]
Evaporation pressure drop	Jung & Radermacher [53]

Table 5 Refrigerant condition for training and testing data set.

		Refrigerant charge in system			
		1.9 kg	2.1 kg	2.3 kg	2.5 kg
Initial evaporator refrigerant in system	30 wt%	Train	Train	-	Train
	50 wt%	Train	Train	-	Train
	60 wt%	-	-	Test	-
	70 wt%	Train	Train	-	Train

4. Results and discussion

4.1 Training data evaluation

Fig. 3 shows the refrigerant distribution dataset prepared for training data. From the results in Fig. 3(a), the total amount of refrigerant dominates the refrigerant mass in a component throughout the operation from startup to shutdown. Moreover, the refrigerant distribution is not monotonically offset but exhibits transient behavior, wherein the proportion of refrigerant residing in the evaporator relative to the total refrigerant dynamically changes. Although the datasets in this study are prepared with the simulation model and they possibly have deviations from the real phenomena, the fluctuation of the refrigerant distribution in the figure is also seen in some previous experimental investigations [13, 14], which support the validity of using the dataset to evaluate the neural network analysis in subsequent sections. Additionally, Fig. 3(b) presents the results based on different initial refrigerant distributions. It can be observed that the evaporator refrigerant mass remains dependent on the initial distribution for approximately the first 500 seconds after system startup. This phenomenon is physically reasonable, corresponding to the system behavior where flows starting from different initial conditions converge to a steady state after sufficient development. Nevertheless, it is noted that the time required for flow development is expected to vary depending on factors such as system size and ambient temperature, which influence the circulation time of the refrigerant through the system. Furthermore, the dataset confirms that the refrigerant distribution exhibits nonlinear time dependency concerning the refrigerant charge and initial refrigerant distribution. This suggests that applying data-driven estimation techniques through a neural network is more efficient in terms of both accuracy and time than attempting a new formulation to estimate refrigerant distribution. Based on these findings, using datasets with refrigerant charges and initial refrigerant distributions for the training the LSTM network allows us to discuss the feasibility of predicting the transient operation of the system.

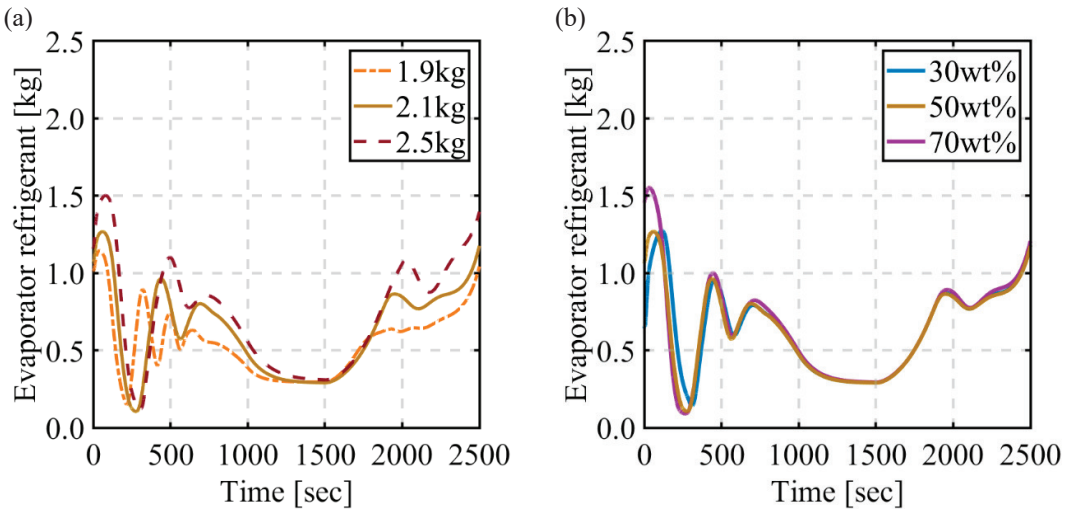

Fig. 3. Sensitivity of evaporator refrigerant transition in the training data toward conditions of (a) charged refrigerant amount under initial refrigerant distribution in the evaporator 50wt%, (b) initial refrigerant distribution in the evaporator at charged refrigerant of 2.1kg.

4.2 Verification of the network

Figure 4 displays plots comparing the predicted and validation data for the basic operational parameters of the heat pump in a scenario with a refrigerant charge of 2.3 kg and initially 60 wt% concentration of refrigerant in the evaporator-a condition that was not included in the training. The

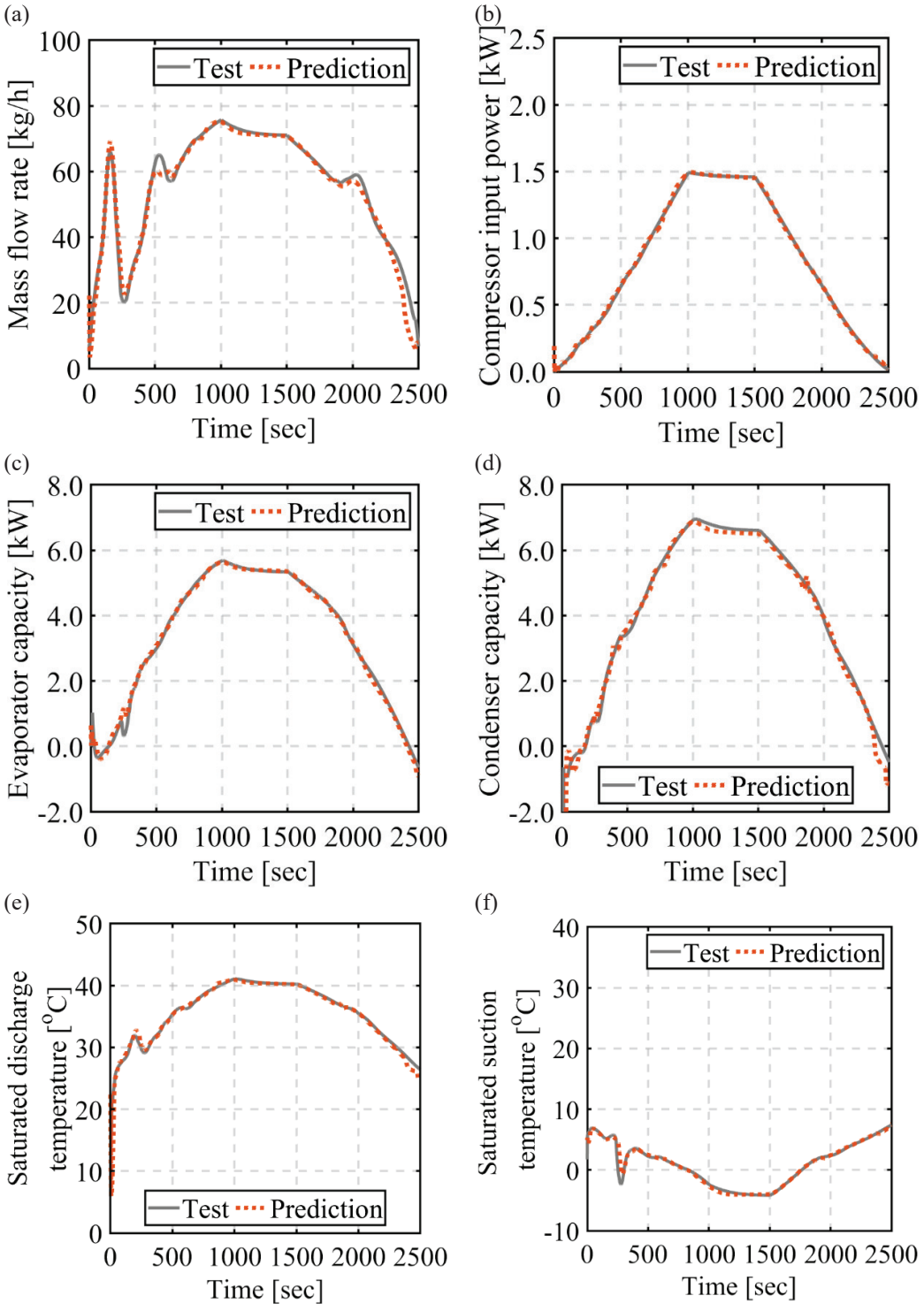

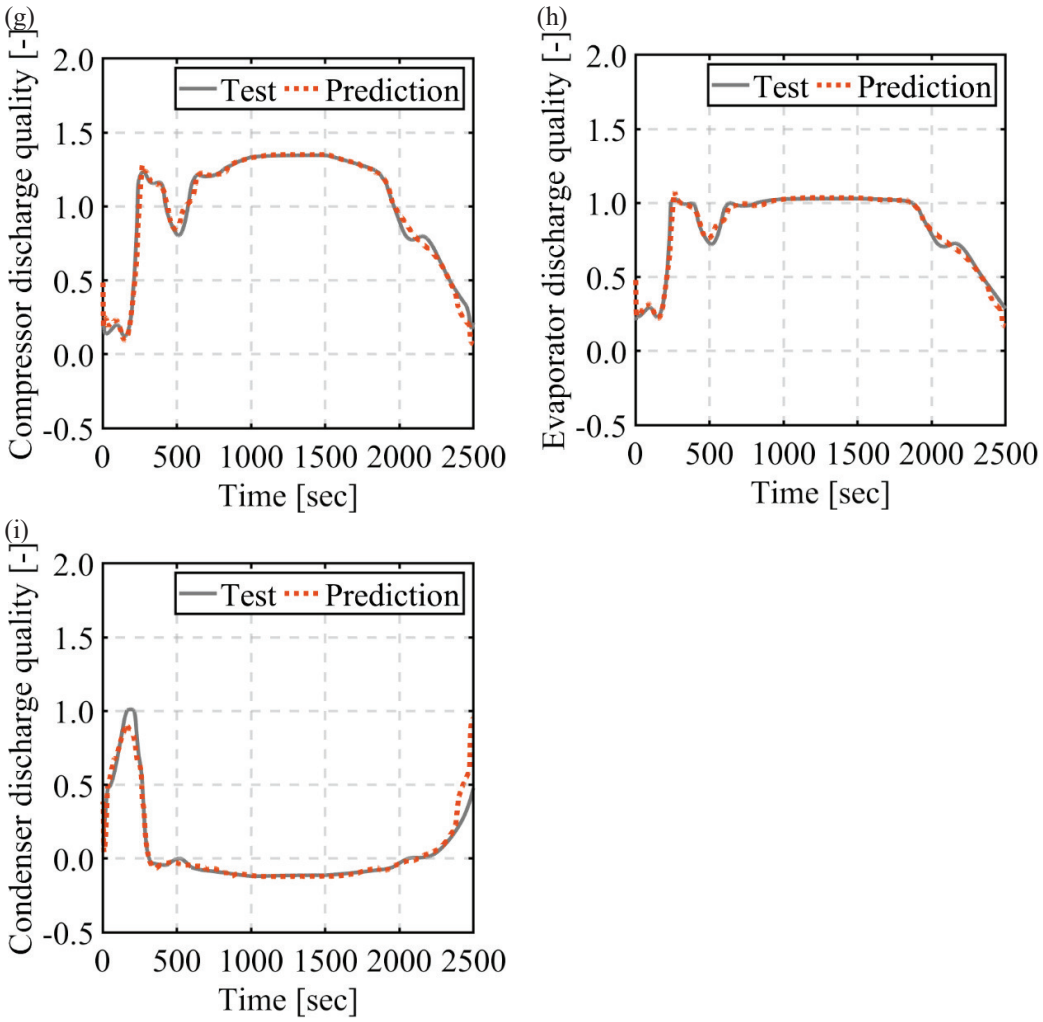

Fig. 4. Validation in the testing condition (refrigerant charge: 2.3 kg, initial refrigerant concentration: 60 wt% in the evaporator) for (a) discharge mass flow rate, (b) compressor power input, (c) evaporator capacity, (d) condenser capacity, (e) saturated discharge temperature, (f) saturated suction temperature, (g) compressor discharge quality, (h) evaporator discharge quality and (i) condenser discharge quality.

phase state of each device, compressor, evaporator and condenser, is represented using a pseudo-quality factor $q(t)$, which is defined by the following equation.

$$q(t) = [H(t) - H_{q=0}(t)]/[H_{q=1}(t) - H_{q=0}(t)]. \quad (4\text{-}1)$$

Here, $H(t)$、$H_{q=0}(t)$、$H_{q=1}(t)$ represent the enthalpy, the saturated liquid enthalpy and the saturated gas enthalpy calculated from the pressure at the subject point, respectively. Although there are occasional absolute deviations, the quantitative agreement between the predictions and the validation data is evident throughout the operation from startup to shutdown. The validation results for refrigerant distribution are shown in Fig. 5. The accuracy for refrigerant distribution was also confirmed to be satisfactory, including the significant oscillations immediately after startup, which

depend on the initial refrigerant distribution. These findings indicate that, given adequate operational

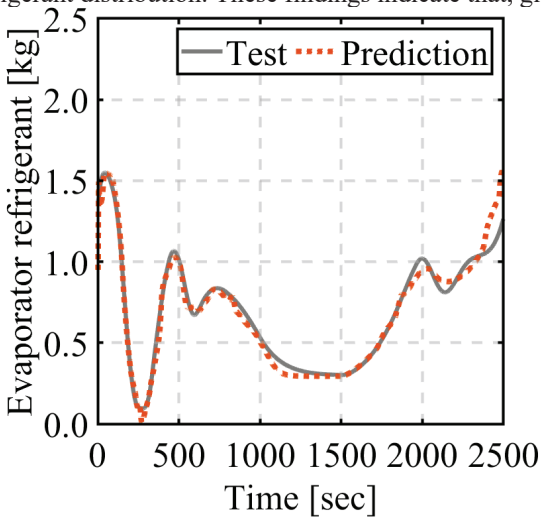

Fig. 5. Validation results in the testing condition (refrigerant charge: 2.3 kg, initial refrigerant concentration: 60 wt% in the evaporator) for refrigerant distribution in the evaporator.

data for various refrigerant charge levels, the model can successfully interpolate to predict conditions for other refrigerant levels and initial refrigerant distributions. This result aligns with the findings of Palagi et al. [23], who demonstrated the effectiveness of LSTM networks over memoryless architectures in capturing long-term dependencies. The computation time required for network training and prediction was 1491 seconds and 0.9553 seconds, respectively, using an Nvidia GeForce RTX 3090 GPU, which is within a practical range for design implementation. Although LSTM networks are known for their comparably higher computational cost [55], we achieved both improved predictive performance and reduced computational load by selecting governing parameters as features based on thermo-fluid dynamics principles and by preparing datasets tailored to the phenomena under investigation [56, 57]. Table 6 lists scale dependent error evaluated by RMSE and DTW. As mentioned in section 2.5, RMSE is highly sensitive to outliers in datasets, which results in a relatively lower prediction accuracy for time-series data. In this point of view, the results obtained from DTW confirm that, due to its characteristic of verifying waveform congruence, the impact of outliers is minimized, resulting in relatively higher accuracy. The non-dimensional accuracy shown in Table 7 summarizes the zero-lag cross-correlation coefficient, the maximum cross-correlation coefficient and its corresponding lag, as well as the coefficient of determination (R^2). All parameters exhibit high correlations, with correlation coefficients exceeding 96% and optimal lag values within ± 3 sec. In general, a Pearson correlation coefficient exceeding 90% is indicative of a very strong positive relationship, [58]. These results confirm that the temporal profiles of the predicted data align very closely with those of the test data. Although R^2 values for prediction in refrigerant distribution is over 95%, one potential factor contributing to the relatively lower value compared to the cross-correlation coefficients is that, by its very formulation, the R^2 metric is sensitive to even a few large errors: thus, the presence of outliers may depress its value. In time-series analysis, achieving a close match in overall trends is generally preferable to precisely predicting a few isolated outliers. Although the above analysis showed good accuracy, the predictive model was constructed solely based on simulation data, and therefore, additional considerations are required to apply the same analysis to experimental data. First, in experimental measurements, it is generally difficult to obtain information within the two-phase region. Furthermore, as mentioned in the Introduction, capturing the transient behavior of refrigerant distribution is inherently challenging. To overcome these limitations, it is necessary to consider techniques such as data assimilation, which supplements sparse measurement data with simulation models, or the incorporation of additional visualization technologies to enhance the accuracy of validation. For instance of visualization technology, the authors are progressing in

elucidating fluid phenomena of zeotropic mixture using optical measuring devices [10]. These approaches enable to reinforce the training data with refrigerant properties, such as two phase enthalpy and composition ratio.

Consequently, a prediction method that is more sensitive to the overall transient behavior is deemed more desirable than one that is overly sensitive to outlier errors. As an alternative evaluation metric, in addition to the cross-correlation function discussed herein, error assessment using the mean squared logarithmic error [59] or other relative measures [60] could also be considered. Moreover, since the training and test data employed in this study were generated from simulation analyses, the high prediction accuracy achieved may be partially attributed to the fact that the simulation data were constructed from combinations of linear models. In contrast, it is well known that actual operational data for two-phase refrigerants in heat pumps frequently exhibit nonlinear phenomena [6-11, 61, 62]; hence, additional ingenuity will be required to achieve similarly high prediction accuracy for such systems.

Table 6 Scale dependent error for the test data.

Output features	Unit	*RMSE*	*DTW*
Mass flow rate	[kg/h]	2.73	2.51×10^{-1}
Compressor power input	[kW]	1.42×10^{-2}	6.25×10^{-4}
Evaporator capacity	[kW]	1.26×10^{-2}	8.56×10^{-3}
Condenser capacity	[kW]	8.12×10^{-1}	3.53×10^{-2}
Saturated discharge temperature	[°C]	1.17	5.49×10^{-2}
Saturated suction temperature	[°C]	5.63×10^{-1}	3.45×10^{-2}
Compressor discharge quality	[-]	4.47×10^{-2}	4.20×10^{-3}
Evaporator discharge quality	[-]	3.26×10^{-2}	3.05×10^{-3}
Condenser discharge quality	[-]	3.26×10^{-2}	7.14×10^{-3}
Evaporator refrigerant	[kg]	6.26×10^{-2}	8.64×10^{-3}
Condenser refrigerant	[kg]	7.11×10^{-2}	1.51×10^{-2}
Gas pipe refrigerant	[kg]	4.82×10^{-3}	6.59×10^{-4}
Liquid pipe refrigerant	[kg]	3.46×10^{-3}	4.89×10^{-4}

Table 7 Dimensionless accuracy for the test data.

Output features	R^2	$CCF_k(0)$	$CCF_{k,max}$	$\tau_{CCF_{k,max}}$
Unit	[%]	[%]	[%]	[sec]
Mass flow rate	97.51	99.10	99.10	0
Compressor power input	99.93	99.96	99.96	0
Evaporator capacity	99.60	99.80	99.80	0
Condenser capacity	90.36	96.00	96.51	2
Saturated discharge temperature	94.09	97.76	97.84	1
Saturated suction temperature	97.41	98.71	98.71	0
Compressor discharge quality	98.63	99.34	99.34	0
Evaporator discharge quality	98.32	99.21	99.21	0
Condenser discharge quality	92.83	96.55	96.55	0
Evaporator refrigerant	96.49	98.54	98.54	0
Condenser refrigerant	95.85	98.79	98.79	0

Gas pipe refrigerant	96.17	98.11	98.12	1
Liquid pipe refrigerant	96.00	98.00	98.00	0

4.3 Spike noise propagation

4.3.1 Evaporator refrigerant sensitivity at specific time during startup

In addition to evaluating accuracy with respect to a specific feature, it is valuable to assess whether the relationships with surrounding features are reasonable from a thermo-fluid perspective. To this end, we injected a spike noise into the evaporator refrigerant quantity at a given time and analyzed the subsequent response. The target data set followed the network's test data, with a refrigerant charge of 2.3 kg and an initial evaporator refrigerant constituting 60wt% of the total system. Figure 6 illustrates the changes and propagation in the evaporator and condenser refrigerant quantities when a noise is applied to the evaporator refrigerant distribution at 500 sec. First, the temporal evolution of the evaporator refrigerant quantity reveals that, after 500 sec, an oscillatory propagation is observed for approximately 50 sec. This behavior is interpreted as follows: a modification in the refrigerant distribution at a specific time alters the condenser refrigerant, in turn changes the refrigerant supply to the evaporator over the subsequent period. Supporting this interpretation, an analysis of the condenser refrigerant shows that, despite some instantaneous outliers, its variation is inversely related to that of the evaporator refrigerant quantity. These observations are consistent with the fundamental mass conservation relationships governing the refrigerant within the system.

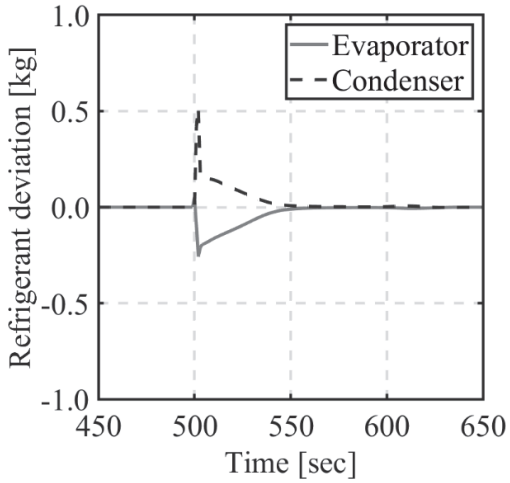

Fig. 6. Sensitivity and Propagation of spike noise at 500 sec on evaporator refrigerant at test data in refrigerant mass of evaporator and condenser.

4.3.2 Discharge quality dependency on evaporator refrigerant in time sequence

Figure 7 compares the cross-correlation coefficients, computed between the compressor discharge quality and the evaporator refrigerant distribution under noise injection, at various time instances. The time points correspond to (a) 50 sec after startup when the compressor frequency is gradually increasing, (b) 500 sec after startup, (c) 1250 sec after startup approximately 4 min after the compressor frequency has reached steady state, and (d) 2000 sec after startup when the compressor frequency is gradually decreasing. In particular at a lag time of 0, the quality of the discharge refrigerant at the compressor exhibits a negative correlation with the evaporator refrigerant quantity− a relationship that is widely recognized among industry practitioners. The sudden increase in evaporator refrigerant reduces the gas ratio of evaporator and suppress suction quality. At the same time, reduction in the suction quality leads to lower suction enthalpy, which subsequently reduces discharge quality of compressor. At each time point, the correlation coefficients exhibit characteristic trends. In (a), an oscillation with a period of about 25 sec is observed in a nearly origin-symmetric pattern. This indicates that the discharge quality also oscillates and interacts mutually with the evaporator refrigerant. The negative correlation between the evaporator refrigerant and the discharge quality can be attributed to the phenomena mentioned above.

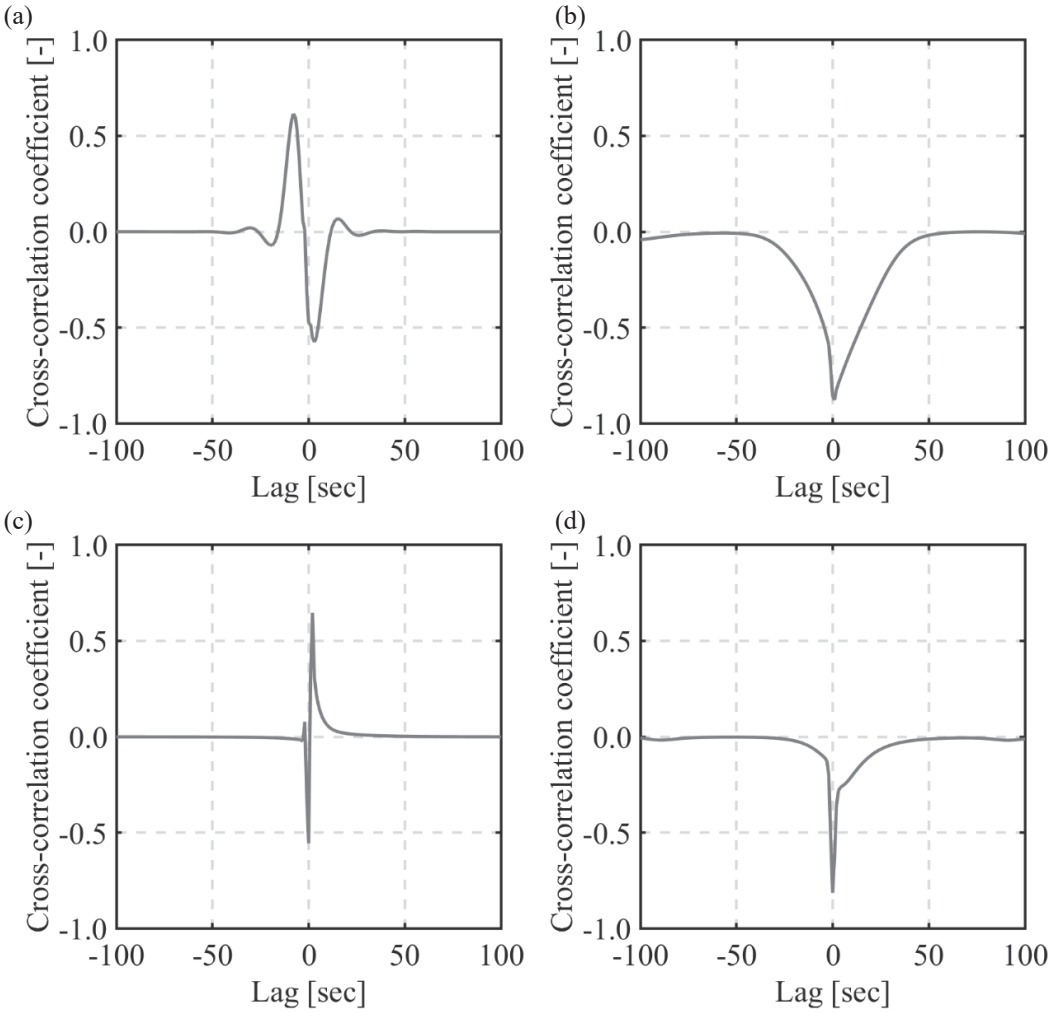

Fig. 7. Correlation analysis of discharge quality dependency on refrigerant amount in evaporator at time (a) 50sec, (b) 500sec, (c) 1250sec and (d) 2000sec.

Moreover, a physical explanation for the rise in the evaporator refrigerant quantity as the discharge quantity increases is that the corresponding increase in refrigerant density supplied to the condenser leads to a higher condenser refrigerant, which, due to mass conservation, results in a reduction in the evaporator refrigerant. The physical implications of the origin-symmetric cross-correlation coefficient have been discussed in previous studies [37]. In the case of (b), the increase in the evaporator refrigerant quantity due to a reduction in the discharge refrigerant is not observed; rather, a strong negative correlation is exhibited. The difference with (a) can be attributed to the absolute value of the discharge quality: while (a) is characterized by a low discharge quality immediately after startup, in (b) the discharge quality is around one, indicating a higher gas content, and hence the reduction in refrigerant density is smaller. For (c), the cross-correlation function shows a rapid oscillatory pattern, with a sharp negative peak followed by a positive peak within a lag of 25 sec at positive lags, rendering the pattern non-symmetric with respect to the origin. This non-symmetry suggests that, as in (b), the sensitivity of the evaporator refrigerant quantity to changes in the discharge quality is small, and the observed oscillation is primarily due to a time delay in the response of the evaporator to variations in discharge dryness. In other words, the phase shift between the oscillations of the evaporator refrigerant quantity and the discharge quality creates a transient period during which a positive correlation might appear. Such a phenomenon has also been reported in [55]. In (d), a sharp negative correlation peak is observed. The presence of this sharp peak indicates that the relatively small, i.e., strong, negative correlation and the short propagation of noise. In summary, RBSA framework enables the sensitivity analysis of operating parameters under small noise loads using cross-correlation functions. This method has demonstrated practical utility in elucidating different phenomena under varying operating conditions and offers promising insights for further investigation.

4.4 Gaussian noise propagation

4.4.1 Evaporator refrigerant sensitivity on variance

As a contrasting approach to the spike noise analysis discussed earlier, this section examines the impact of introducing continuous white noise into the system. In particular, prior studies have revealed that two-phase flow behaviors inherently exhibit variability [63, 64], which constitutes a key discrepancy between experimental observations and conventional numerical analyses. Several factors contribute to the variability observed in two-phase flow, including the oscillatory nature of the flow itself [65] and the highly complex and dissipative mechanisms associated with liquid droplets within the flow [66]. Instead of explicitly modeling these complex phenomena, this study focuses on the dominant influence of refrigerant distribution across various operating parameters, as observed in previous analysis. Specifically, we investigate the propagation of operational data fluctuations arising from variations in refrigerant distribution. Figure 8 presents the results of an analysis in which white

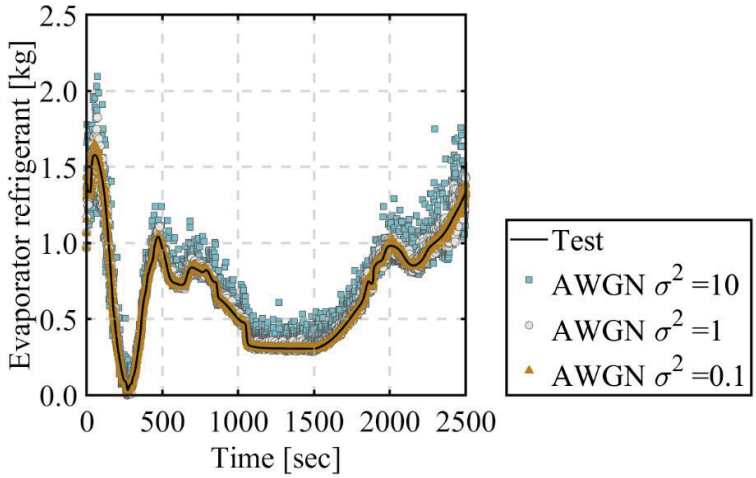

Fig. 8. Variability estimation of refrigerant distribution in evaporator under additive white Gaussian noise (AWGN) variance σ^2 of, 0.1, 1, 10.

noise−characterized by a specified variance−was added to the predicted evaporator refrigerant quantity at each time step, and the resulting propagation effects were assessed. Notably, the applied noise was not isolated to individual time steps but rather incorporated the cumulative influence of propagated noise from preceding time steps. As illustrated in Fig. 8, the amplitude of variability changes as a function of variance in evaporator refrigerant. When the variance is set to 0.1, the fluctuations remain minimal, whereas at a variance of 10, the noise becomes significant, leading to a noticeable deviation of the mean refrigerant quantity from the original dataset. This behavior aligns with response trends governed by the signal-to-noise (S/N) ratio in stochastic resonance. While it might be pointed out that the noise-applied datasets exhibit generally higher values than the test data, particularly for the case with a variance of 10, this behavior can be attributed to the inherent pressure differences between the evaporator and condenser. Although Gaussian noise was probabilistically added to the refrigerant mass, the resulting flow dynamics are influenced by the pressure gradient between the components. Additional refrigerant introduced into the evaporator is more likely to remain within the device, given its position at a lower pressure state within the refrigerant cycle. Conversely, a reduction in the refrigerant mass within the evaporator, accompanied by an increase in refrigerant mass within the condenser−where the system pressure is comparatively higher−tends to promote refrigerant flow from the condenser back to the evaporator, following the natural pressure gradient. The predicted variability at a variance of 1 is 8.9%, which closely aligns with the approximately 10% variability reported in previous study [64]. Based on this observation, the subsequent section evaluates the propagation effects of noise variance 1 on other operating parameters.

4.4.2 Operational sensitivity on evaporator refrigerant variance

Figure 9 illustrates the variability of system operating parameters as influenced by fluctuations in evaporator refrigerant quantity. A key point to emphasize is that the Gaussian noise in this analysis was not independently added to each parameter; rather, it was introduced solely into the refrigerant distribution within the evaporator, and the resulting impact on operating parameters was subsequently visualized. Representative variation ranges during operation of fixed compressor frequency in 1000sec to 1500sec are as follows: 5.5% in mass flowrate, 6.1% in compressor input 5.5% in evaporator capacity and 9.9% in condenser capacity. These results indicate that fluctuations in refrigerant distribution propagate sufficiently to operating parameters, making them measurable within a practical range. This suggests that operating parameter measurements may support to infer refrigerant distribution, thereby offering a potential methodology for indirect estimation. This finding is particularly significant for the future application of the proposed analytical technique in experimental evaluations. One aspect that warrants further investigation is the transient variation in distribution variance. In this work, a uniform variance was applied as a preliminary validation step. However, transient states may exhibit different fluctuation characteristics compared to steady-state operation. By further examining such scenarios, a more comprehensive understanding of refrigerant distribution can be achieved. Moreover, the dynamic influence of actuator-induced perturbations would occur in the real system. These undesigned cause of refrigerant fluctuation should be kept in mind to improve durability of the system. Future investigation will take this real-world noise into perspective.

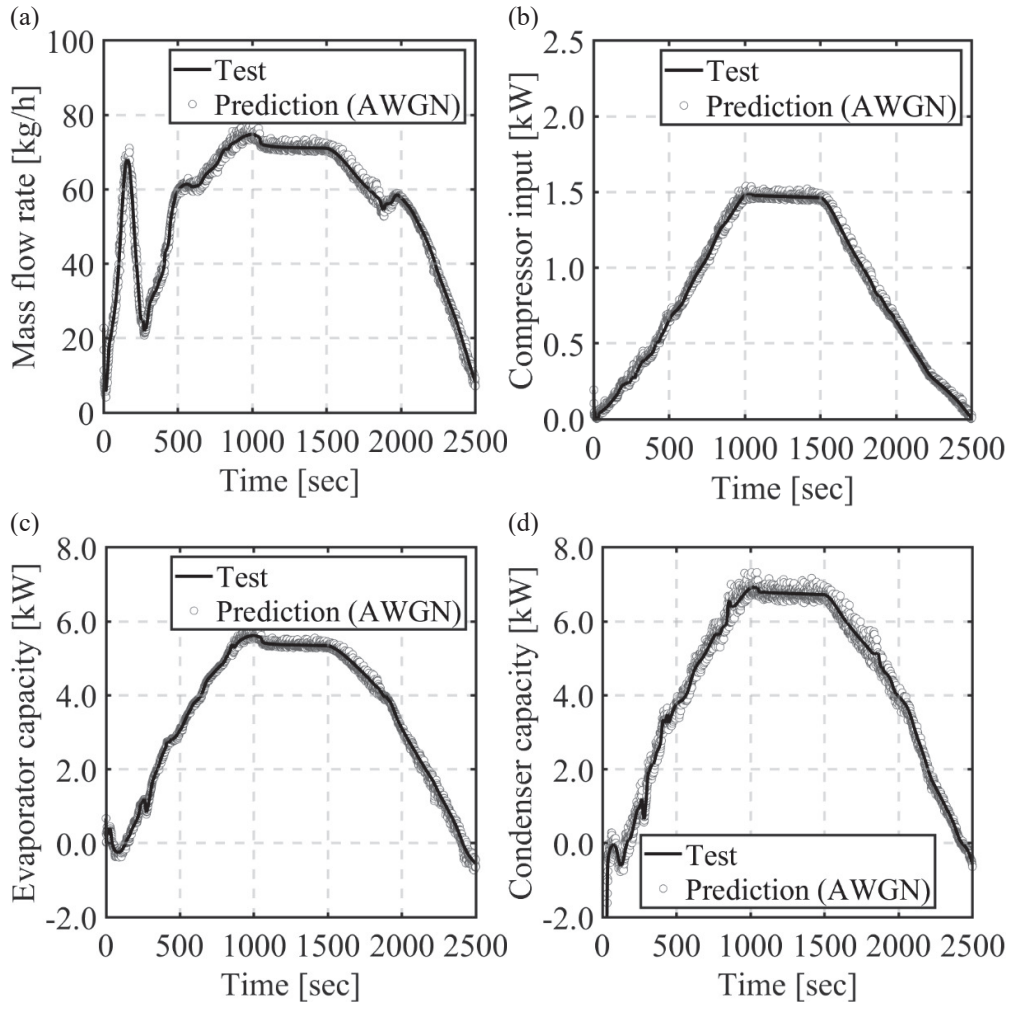

Fig. 9. Propagation of additive white Gaussian noise (AWGN) in evaporator refrigerant for (a) discharge mass flow rate, (b) compressor power input, (c) evaporator capacity, (d) condenser capacity.

5. Conclusions

In this study, we examined the applicability of an LSTM-based analytical technique in a heat pump system. The main conclusions in this study are as follows:

(1) The network using operational data incorporating refrigerant distribution enables accurate prediction. The training dataset included initial refrigerant distributions in the evaporator at 30 wt%, 50 wt%, and 70 wt%, along with three levels of total refrigerant charge. The results confirmed that the network successfully predicts transient refrigerant distribution for untrained initial evaporator refrigerant distribution and charge level with an accuracy over 95%.

(2) Resonance-Based Sensitivity Analysis (RBSA) attracted by the stochastic resonance-like behavior of LSTM evaluates the influence intensity and propagation time of feature perturbations introduced through noise injection into the network. By analyzing feature interactions via cross-correlation functions, we demonstrated that the proposed approach aligns with established heat pump system knowledge, providing a reliable framework for sensitivity assessment.

(3) Transient variations in refrigerant distribution variance are examined, revealing that fluctuations in the distributions have a notable impact on operational parameters. From the experimental literature, we selected the value of 1 as a practical variance and its impact on condenser capacity went up to variation of 10% under fixed control. These findings contribute to understanding refrigerant dynamics and provide a foundation for robust and resilient designs.

The applicability of an LSTM-based analytical technique was examined in this study based on simulation data. Future research will focus on addressing the prediction accuracy degradation caused by various types of noise, including meaningful noise based on the fluid transportation phenomena and meaningless noise resulting from measurement errors, as well as on elucidating non-modeled phenomena that become evident in real experimental scenarios. Methods to suppress the reduction in prediction accuracy due to these noises and to clarify the unexplained phenomena present in the model are of particular interest. Moreover, this methodology is not limited to heat pump applications; it has the potential to be extended to the design of various energy systems utilizing transient working fluids, as well as the analysis of cyclic systems, including biological circulatory processes. Future advancements in this analytical approach hold promise for broader applications in both engineering and scientific research.

Declaration of Generative AI and AI-assisted technologies in the writing process

During the preparation of this work the authors used ChatGPT in order to improve the language and grammar. After using this tool, the authors reviewed and edited the content as needed and take full responsibility for the content of the publication.

References

[1] IRENA International Renewable Energy Agency. "Power to Heat and Cooling: Status." (n.d.). Available at: https://www.irena.org/Innovation-landscape-for-smart-electrification/Power-to-heat-and-cooling/Status (Accessed February 16, 2025).

[2] Eurostat. "Energy Consumption in Households." Report by Eurostat, Luxembourg, 1993. Available at: https://ec.europa.eu/eurostat/statistics-explained/SEPDF/cache/58200.pdf (Accessed April 8, 2025).

[3] Kuntuarova S., Licklederer T., Huynh T., Zinsmeister D., Hamacher T., Peri´c V. "Design and Simulation of District Heating Networks: A Review of Modeling Approaches and Tools." Energy, vol. 305, 2024, article 132189. https://doi.org/10.1016/j.energy.2024.132189.

[4] Vering C., Maier L., Breuer K., Krützfeldt H., Streblow R., Müller D. "Evaluating Heat Pump System Design Methods Towards a Sustainable Heat Supply in Residential Buildings." Applied Energy, vol. 308, 2022, 118204. https://doi.org/10.1016/j.apenergy.2021.118204.

[5] Malhotra M., Li Z., Liua X., Lapsa M., Bouza T., Vineyard E. "Heat Pumps in the United States: Market Potentials, Challenges and Opportunities, Technology Advances." Proceedings of the 14th IEA Heat Pump Conference, Chicago, USA, May 15-18, 2023. https://doi.org/10.23697/xad4-dh11.

[6] Pons M., Delahaye A., Fournaison L., Dalmazzone D. "Energy Analysis of Two-Phase Secondary Refrigeration in Steady-State Operation, Part 2: Exergy Analysis and Effects of Phase Change Kinetics." Energy, vol. 161, 2018, pp. 1291-1299. https://doi.org/10.1016/j.energy.2018.07.044.

[7] Thome J.R., Dupont V., Jacobi A.M. "Heat Transfer Model for Evaporation in Microchannels. Part I: Presentation of the Model." International Journal of Heat and Mass Transfer, vol. 47, no. 16, 2004, pp. 3375-3385. https://doi.org/10.1016/j.ijheatmasstransfer.2004.01.006.

[8] Onaka Y., Miyara A., Tsubaki K. "Experimental Study on Evaporation Heat Transfer of CO_2/DME Mixture Refrigerant in a Horizontal Smooth Tube." International Journal of Refrigeration, vol. 33, no. 7, 2010, pp. 1277-1291. https://doi.org/10.1016/j.ijrefrig.2010.06.014.

[9] Li J., Hrnjak P. "Optimization of a Microchannel Condenser with Separation Circuitry." Applied Thermal Engineering, vol. 184, 2021, article 116273. https://doi.org/10.1016/j.applthermaleng.2020.116273.

[10] Miyawaki K., Shikazono N. "Dynamic Evaluation of Circulation Composition of Zeotropic Refrigerant in Heat Pump System with NIR Absorption Spectroscopy." International Refrigeration and Air Conditioning Conference, 2024, Paper 2599. https://docs.lib.purdue.edu/iracc/2599.

[11] Jouhara H., Abnieska-Góra A., Delpech B., Olabi V., el Samad T., Sayma A. "High-Temperature Heat Pumps: Fundamentals, Modelling Approaches and Applications." Energy, vol. 303, 2024, article 131882. https://doi.org/10.1016/j.energy.2024.131882.

[12] Poggi F., Macchi-Tejeda H., Leducq D., Bontemps A. "Refrigerant Charge in Refrigerating Systems and Strategies of Charge Reduction." International Journal of Refrigeration, vol. 31, no. 3, 2008, pp. 353-370. https://doi.org/10.1016/j.ijrefrig.2007.05.014.

[13] Li B., Peuker S., Hrnjak P.S., Alleyne A.G. "Refrigerant Mass Migration Modeling and Simulation for Air Conditioning Systems." Applied Thermal Engineering, vol. 31, no. 10, 2011, pp. 1770-1779. https://doi.org/10.1016/j.applthermaleng.2011.02.022.

[14] Han B., Yan G., Yu J. "Refrigerant Migration During Startup of a Split Air Conditioner in Heating Mode." Applied Thermal Engineering, vol. 148, 2019, pp. 1068-1073. https://doi.org/10.1016/j.applthermaleng.2018.11.126.

[15] Qiao H., Laughman C. "Dynamic Modeling of Oil Transport in Vapor Compression Systems." International Refrigeration and Air Conditioning Conference, 2022, Paper 2352. https://docs.lib.purdue.edu/iracc/2352.

[16] Fukuda S., Takata N., Koyama S. "The Circulation Composition Characteristic of the Zeotropic Mixture R1234ze(E)/R32 in a Heat Pump Cycle." International Refrigeration and Air Conditioning Conference, 2012, Paper 2229. https://docs.lib.purdue.edu/iracc/1221/.

[17] Ling J., Qiao H., Alabdulkarem A., Aute V., Radermacher R. "Modelica-Based Heat Pump Model for Transient and Steady-State Simulation Using Low-GWP Refrigerants." International Refrigeration and Air Conditioning Conference, 2014, Paper 1421. http://docs.lib.purdue.edu/iracc/1421.

[18] Kia M., Nazar M.S., Sepasian M.S., Heidari A., Siano P. "An Efficient Linear Model for Optimal Day-Ahead Scheduling of CHP Units in Active Distribution Networks Considering Load Commitment Programs." Energy, vol. 139, 2017, pp. 798-817. https://doi.org/10.1016/j.energy.2017.08.008.

[19] Niu D., Ji Z., Li W., Xu X., Liu D. "Research and Application of a Hybrid Model for Mid-Term Power Demand Forecasting Based on Secondary Decomposition and Interval Optimization." Energy, vol. 234, 2021, article 121145. https://doi.org/10.1016/j.energy.2021.121145.

[20] Bechtler H., Browne M.W., Bansal P.K., Kecman V. "Neural Networks: A New Approach to Model Vapour-Compression Heat Pumps." International Journal of Energy Research. https://doi.org/10.1002/er.705.

[21] Dengiz, T., Kleinebrahm, M. "Imitation Learning with Artificial Neural Networks for Demand Response with a Heuristic Control Approach for Heat Pumps." Energy and AI, vol. 18, Dec. 2024, article 100441. https://doi.org/10.48550/arXiv.2407.11561.

[22] Hochreiter, S., Schmidhuber, J. "Long Short-Term Memory." Neural Computation, vol. 9, no. 8, 1997, pp. 1735–1780. https://doi.org/10.1162/neco.1997.9.8.1735.

[23] Palagi, L., Pesyridis, A., Sciubba, E., Tocci, L. "Machine Learning for the Prediction of the Dynamic Behavior of a Small-Scale ORC System." Energy, vol. 166, 2019, pp. 72-82. https://doi.org/10.1016/j.energy.2018.10.059.

[24] Laib, O., Khadir, M. T., Mihaylova, L. "Toward Efficient Energy Systems Based on Natural Gas Consumption Prediction with LSTM Recurrent Neural Networks." Energy, vol. 177, 2019, pp. 530-542. https://doi.org/10.1016/j.energy.2019.04.075.

[25] Bouziane, S. E., Khadir, M. T. "Towards an Energy Management System Based on a Multi-Agent Architecture and LSTM Networks." Journal of Experimental & Theoretical Artificial Intelligence, vol. 36, no. 4, 2024, pp. 469-487. https://doi.org/10.1080/0952813X.2022.2093407.

[26] Lyu, Z., Wang, Y., Sciazko, A., Li, H., Komatsu, Y., Sun, Z., Sun, K., Shikazono, N., Han, M. "Prediction of Fuel Cell Performance Degradation Using a Combined Approach of Machine Learning and Impedance Spectroscopy." Journal of Energy Chemistry, vol. 87, Dec. 2023, pp. 32-41. https://doi.org/10.1016/j.jechem.2023.08.028.

[27] Zou, Z., Yu, X., Ergan, S. "Towards Optimal Control of Air Handling Units Using Deep Reinforcement Learning and Recurrent Neural Network." Building and Environment, vol. 168, 2020, article 106535. https://doi.org/10.1016/j.buildenv.2019.106535.

[28] Lahariya, M., Karami, F., Develder, C., Crevecoeur, G. "Physics-Informed LSTM Network for Flexibility Identification in Evaporative Cooling Systems." IEEE Transactions on Industrial Informatics, vol. 19, no. 2, 2022. https://doi.org/10.1109/TII.2022.3173897.

[29] Kong, W., Dong, Z. Y., Jia, Y., Hill, D. J., Xu, Y., Zhang, Y. "Short-Term Residential Load Forecasting Based on LSTM Recurrent Neural Network." IEEE Transactions on Smart Grid, vol. 10, no. 1, 2019, p. 841. https://doi.org/10.1109/TSG.2017.2753802.

[30] Eom, Y. H., Chung, Y., Park, M., Hong, S. B., Kim, M. S.
"Deep Learning-Based Prediction Method on Performance Change of Air Source Heat Pump System Under Frosting Conditions."
Energy, vol. 228, 2021, article 12054. https://doi.org/10.1016/j.energy.2021.120542.

[31] Jeong, G., Lee, J. H., Choi, H. W., Park, H. W., Kim, H. J., Seo, B. S., Chin, S.
"Deep Learning-Based Prediction of Oil Reversal in R290 Heat Pump Systems."
Energy, vol. 320, Apr. 1, 2025, article 135255. https://doi.org/10.1016/j.energy.2025.135255.

[32] Mehdi, S., Tiwary, P. “Thermodynamics-inspired explanations of artificial intelligence.” Nature Communications vol. 15, 2024, 7859. https://doi.org/10.1038/s41467-024-51970-x

[33] Hülsmann, J., Barbosa, J., Steinke, F. “Local Interpretable Explanations of Energy System Designs”. Energies vol. 16, no. 5, 2023, 2161. https://doi.org/10.3390/en16052161.

[34] Vera-Piazzini, O., Scarpa, M., “Building energy model calibration: a review of the state of the art in approaches, methods, and tools” Journal of Building Engineering. vol. 86, 2023, 108287, https://doi.org/10.1016/j.jobe.2023.108287.

[35] von Rueden, L., et al. "Informed Machine Learning – A Taxonomy and Survey of Integrating Prior Knowledge into Learning Systems." IEEE Transactions on Knowledge and Data Engineering, vol. 33, no. 6, 2021, pp. 2347–2362. https://doi.org/10.1109/TKDE.2021.3079836.

[36] Wiesenfeld, K., Moss, F. "Stochastic Resonance and the Benefits of Noise: From Ice Ages to Crayfish and SQUIDs." Nature, vol. 373, 1995, pp. 33–36. https://doi.org/10.1038/373033a0.

[37] Gammaitoni, L., Hänggi, P., Jung, P., Marchesoni, F. "Stochastic Resonance." Reviews of Modern Physics, vol. 70, 1998, p. 223–287. https://doi.org/10.1103/RevModPhys.70.223.

[38] Faisal, A. A., Selen, L. P., Wolpert, D. M. "Noise in the Nervous System." Nature Reviews Neuroscience, vol. 9, no. 4, 2008, pp. 292–303. https://doi.org/10.1038/nrn2258.

[39] Stein, R. B., et al.
"Neuronal Variability: Noise or Part of the Signal?"
Nature Reviews Neuroscience, vol. 6, no. 5, 2005, pp. 389–397. https://doi.org/10.1038/nrn1668

[40] McDonnell, M. D., Abbott, D.
"What is Stochastic Resonance? Definitions, Misconceptions, Debates, and Its Relevance to Biology."
Nature Reviews Neuroscience, vol. 10, 2009, pp. 415–423.
https://doi.org/10.1371/journal.pcbi.1000348

[41] Kingma, D., Ba, J.
"Adam: A Method for Stochastic Optimization."
Proceedings of the 3rd International Conference on Learning Representations, USA, 2015.
https://doi.org/10.48550/arXiv.1412.6980

[42] MathWorks.
"TrainingOptionsADAM." [Online]. Available at:
https://jp.mathworks.com/help/deeplearning/ref/nnet.cnn.trainingoptionsadam.html#responsive_offcanvas (Accessed April 2025).

[43] Smith, L. N.
"Cyclical Learning Rates for Training Neural Networks."
IEEE Winter Conference on Applications of Computer Vision, USA, 2017.
https://doi.org/10.1109/WACV.2017.58

[44] MathWorks.
"Deep Learning Toolbox." [Online]. Available at: https://www.mathworks.com/help/deeplearning/ (Accessed April 2025).

[45] Sakoe, H., and Chiba, S.
"Dynamic Programming Algorithm Optimization for Spoken Word Recognition."
IEEE Transactions on Acoustics, Speech, and Signal Processing. Vol. ASSP-26, No. 1, 1978, pp. 43–49. https://doi.org/10.1109/TASSP.1978.1163055.

[46] Qiao, H., Aute, V., Radermacher, R.
"Transient Modeling of a Flash Tank Vapor Injection Heat Pump System – Part I: Model Development."
International Journal of Refrigeration, vol. 49, 2015, pp. 169–182.
https://doi.org/10.1016/j.ijrefrig.2014.06.019

[47] Qiao, H., Laughman, C. R., Burns, D., Bortoff, S.
"Dynamic Characteristics of an R410-A Multi-Split Variable Refrigerant Flow Air-Conditioning System."
12th IEA Heat Pump Conference, Rotterdam, 2017. [Online].
https://heatpumpingtechnologies.org/publications/p-3-1-4-dynamic-characteristics-of-an-r-410a-multi-split-variablerefrigerant-flow-air-conditioning-system/ (Accessed April 2025).

[48] Dittus, F.W., Boelter, L.M.K.,
“Heat Transfer in Automobile Radiators of the Tubular Type.”
International Communications in Heat and Mass Transfer, vol. 12, 1985, pp. 3-22.
https://doi.org/10.1016/0735-1933(85)90003-X

[49] Dobson, M. K., Chato, J. C., “Condensation in Smooth Horizontal Tubes.”
Journal of Heat Transfer, vol. 120, no.1, 1998, pp. 193-213.
https://doi.org/10.1115/1.2830043

[50] Gungor, K.E., Winterton, R.H.S.,
“A general correlation for flow boiling in tubes and annuli.”
International Journal of Heat and Mass Transfer, vol. 29, no.3, 1986, pp.351–358.
https://doi.org/10.1016/0017-9310(86)90205-X

[51] Incropera, F.P. and DeWitt, D.P.,
“Introduction to heat transfer” (3rd Ed.). John Wiley & Sons, 1996, New York.

[52] Lockhart, R.W. and Martinelli, R.C.,
“Proposed correlation of data for isothermal two-phase, two-component flow in pipes.”
Chemical Engineering Progress, vol. 45, no.1, 1949, pp. 39-48.

[53] Jung, D. S., McLinden, M., Radermacher, R., Didion, D.,
“A study of flow boiling heat transfer with refrigerant mixtures.”
International Journal of Heat and Mass Transfer, vol. 32, no.9, 1989, pp. 1751-1764.

[54] Dassault Systemes AB, Dymola. 2023.
[Online]. Available at: https://www.3ds.com/ (Accessed April 2025).

[55] Dey, R., Salem, F. M.
"Gate-Variants of Gated Recurrent Unit (GRU) Neural Networks."
2017 IEEE 60th International Midwest Symposium on Circuits and Systems (MWSCAS), 2017. https://doi.org/10.1109/MWSCAS.2017.8053243

[56] Schmid, P. J., Sesterhenn, J.
"Dynamic Mode Decomposition of Numerical and Experimental Data."
61st Annual Meeting of the APS Division of Fluid Dynamics, American Physical Society, College Park, MD, 2008. https://doi.org/10.1017/S0022112010001217.

[57] Taira, K., Brunton, S. L., Dawson, S. T., Rowley, C. W., Colonius, T., McKeon, B. J., et al.
"Modal Analysis of Fluid Flows: An Overview."
AIAA Journal, vol. 55, no. 12, 2017, pp. 4013–4041. https://doi.org/10.2514/1.J056060.

[58] Cohen, J.
"A Power Primer."
Psychological Bulletin, vol. 112, no. 1, 1992, pp. 155–159. https://doi.org/10.1037/0033-2909.112.1.155

[59] Hodson, T. O., Over, T. M., Foks, S. S.
"Mean Squared Error, Deconstructed."
Journal of Advances in Modeling Earth Systems, vol. 13, no. 12, 2021, article e2021MS002681. https://doi.org/10.1029/2021MS002681

[60] Hyndman, R. J., Koehler, A. B.
"Another Look at Measures of Forecast Accuracy."
International Journal of Forecasting, vol. 22, 2006, pp. 679–688. https://doi.org/10.1016/j.ijforecast.2006.03.001

[61] Giannetti, N., Yamaguchi, S., Saito, K.
"Numerical Simulation of Marangoni Convection within Absorptive Aqueous Li-Br."
International Journal of Refrigeration, vol. 92, Aug. 2018, pp. 176–184. https://doi.org/10.1016/j.ijrefrig.2018.05.035

[62] Moss, F., Ward, L. M., Sannita, W. G.
"Stochastic Resonance and Sensory Information Processing: A Tutorial and Review of Application."
Clinical Neurophysiology, vol. 115, no. 2, 2004, pp. 267–281. https://doi.org/10.1016/S1388-2457(03)00170-6

[63] Wu, J., Tremea, B., Terrier, M.-F., Charni, M., Gagnière, E., Couenne, F., Hamroun, B., Jallut, C.
"Experimental Investigation of the Dynamic Behavior of a Large-Scale Refrigeration – PCM Energy Storage System: Validation of a Complete Model."
Energy, vol. 116, 2016, pp. 32–42. https://doi.org/10.1016/j.energy.2016.09.098

[64] Peuker, S., Hrnjak, P. S.
"Transient Refrigerant Migration and Oil Distribution of an R134a Automotive A/C System."
SAE International Journal of Passenger Cars - Mechanical Systems, vol. 2, no. 1, 2009, pp. 714–724. https://doi.org/10.4271/2009-01-0534

[65] Taitel, Y., Dukler, A. E.
"A Model for Slug Frequency During Gas-Liquid Flow in Horizontal and Near Horizontal Pipes."

International Journal of Multiphase Flow, vol. 3, no. 6, Dec. 1977, pp. 585–596.
https://doi.org/10.1016/0301-9322(77)90031-3

[66] Prosperetti, A., Oguz, H. N.
"The Impact of Drops on Liquid Surfaces and the Underwater Noise of Rain."
Annual Review of Fluid Mechanics, vol. 25, 1993, pp. 577–602.
https://doi.org/10.1146/annurev.fl.25.010193.003045